

Thermal ion kinetic effects and Landau damping in fishbone modes

Chang Liu^{1†}, Stephen C. Jardin¹, Jian Bao², Nikolai Gorelenkov¹,
Dylan P. Brennan¹, James Yang¹, and Mario Podesta¹

¹Princeton Plasma Physics Laboratory, Princeton, NJ 08540, USA

²Institute of Physics, Chinese Academy of Sciences, Beijing 100190, China

(Received xx; revised xx; accepted xx)

The kinetic-MHD hybrid simulation approach for macroscopic instabilities in plasmas can be extended to include the kinetic effects of both thermal ions and energetic ions. The new coupling scheme includes synchronization of density and parallel velocity between thermal ions and MHD, in addition to pressure coupling, to ensure the quasineutrality condition and avoid numerical errors. The new approach has been implemented in the kinetic-MHD code M3D-C1-K, and was used to study the thermal ion kinetic effects and Landau damping in fishbone modes in both DIII-D and NSTX. It is found that the thermal ion kinetic effects can cause an increase of the frequencies of the non-resonant $n = 1$ fishbone modes driven by energetic particles for $q_{\min} > 1$, and Landau damping can provide additional stabilization effects. A nonlinear simulation for $n = 1$ fishbone mode in NSTX is also performed, and the perturbation on magnetic flux surfaces and the transport of energetic particles are calculated.

1. Introduction

The kinetic effects of thermal ions can become more important for physics studies targeting fusion reactors, given the large ion temperature ($T_i > 10$ keV) and the presence of high-energy alpha particles. In recent DIII-D experiments, it was observed that thermal ions can drive both high-frequency chirping modes (Du *et al.* 2021) and beta-induced Alfvén-acoustic eigenmodes (BAAEs)/low-frequency Alfvén modes (Gorelenkov *et al.* 2009; Choi *et al.* 2021; Ma *et al.* 2021). These modes can lead to degradation of plasma confinement or even minor disruption. It is therefore necessary to incorporate these effects in numerical simulation models for ITER and future reactors.

However, the inclusion of thermal ion kinetic effects poses a challenge to classical hybrid simulation models (Todo & Sato 1998; Fu *et al.* 2006; Kim 2008), which combine particle-in-cell (PIC) and the magnetohydrodynamics (MHD) simulations. These models were developed for simulating the physics of energetic particles (EPs) or fast ions, which come from neutral beam injection. EPs can have pressure or perpendicular current that is comparable to the thermal ions or electrons, but their density or momentum are often relatively small compared to the thermal ions. Their kinetic effects can then be included in the MHD framework through pressure or current coupling, by including the $-\nabla \cdot \mathbf{P}$ or $\mathbf{J} \times \mathbf{B}$ term in the momentum equation, where \mathbf{P} and \mathbf{J} are calculated from EP moments.

There are two major issues when extending this approach to thermal ions. First, since the MHD density and momentum equation are derived by taking moments of ion and electron kinetic equations, when thermal ion kinetic equations are calculated separately, these MHD equations become redundant and the error between the two approaches

† Email address for correspondence: cliu@pppl.gov

can lead to numerical issues or even parasitic modes. Second, as ions and electrons are calculated separately (one as kinetic particles and one as a fluid component), the parallel electric force between them must be calculated as a connection, which is often missing in ideal MHD calculations or treated as a high-order two-fluid effect.

In this paper, we describe a new kinetic-MHD coupling scheme, which is similar to the one used in the MEGA code for studying thermal ion kinetic effects in Large Helical Device (LHD) plasmas (Sato & Todo 2019, 2020). In this scheme in addition to the coupling terms in the MHD momentum equation, we have two more equations to connect the MHD and kinetic parts. One is the synchronization of the parallel velocity between the kinetic ions and the MHD, and the other is the synchronization of ion density. These two new equations are introduced to ensure quasi neutrality and avoid parasitic modes.

In this kinetic-MHD model, all the ions, including the thermal ones and the fast ones, are modeled as kinetic particles using the PIC method. The MHD equation is in charge of calculating the evolution of fields and the electron pressure and temperature. The parallel electric field caused by separation of electrons and ions is also added in the ion kinetic equations. This scheme is implemented in the kinetic-MHD code M3D-C1-K (Liu *et al.* 2022), which is based on the finite-element MHD code M3D-C1 (Ferraro & Jardin 2009; Jardin *et al.* 2012). It is found that the semi-implicit method introduced for solving MHD equations (Jardin *et al.* 2012) is helpful for stabilizing numerical instabilities after including ion kinetic terms, and the simulation can run with large timesteps to save computation time.

Using this new model, we investigate the kinetic effects of thermal ions, especially Landau damping, in the kinetic MHD simulations. We first tested the new simulation model in an ion acoustic wave (IAW) simulation, and achieved good agreement of mode frequency and damping rate with the theory. We then studied $n = 1$ fishbone modes using DIII-D and NSTX equilibrium with q_{\min} slightly larger than 1. This fishbone mode which is connected to the non-resonant (1,1) kink mode has been studied before using kinetic-MHD simulation without thermal ion kinetic effects (Brennan *et al.* (2012); Wang *et al.* (2013); Shen *et al.* (2017, 2020)).

We find that for simulation with only fast ions treated kinetically, the dominant $n = 1$ mode has a transition from a classical fishbone mode to a beta-induced Alfvén eigenmode (BAE) like mode as q_{\min} increases, with a significant increase of mode frequency, which is consistent with the NIMROD simulation results (Brennan *et al.* (2012)). After adding a kinetic treatment of the thermal ions, the frequencies of the fishbone modes increase and the growth rates decrease. The BAE-like mode branch becomes stable. These simulation results indicate that both of the two modes are strongly affected by the Landau damping effect from thermal ions which was not considered in previous kinetic-MHD simulations. In addition, we did the nonlinear simulation for the fishbone mode to study the mode saturation and the effects on particle transport.

The paper is organized as follows. In Sec. 2 we discuss the kinetic-MHD coupling scheme including the thermal ions, with density and parallel velocity synchronization. In Sec. 3 we present the simulation results of IAWs using the new scheme, and compare the Landau damping rates with theoretical results. In Sec. 4 we show the numerical simulation of $n = 1$ fishbone modes in a DIII-D equilibrium without and with the thermal ions kinetic effects. In Sec. 5 we did similar simulations in NSTX scenarios, using a more realistic EP distribution. In Sec. 6 we show the results of a nonlinear simulation of fishbones in NSTX, focusing on the mode saturation behavior. Finally, the summary is given in Sec. 7.

2. Kinetic-MHD model with thermal ion kinetic effects

In this section we present the kinetic-MHD model implemented in the M3D-C1-K code. The code was initially developed as a kinetic module for the extended MHD code M3D-C1(Jardin *et al.* 2012) using a pressure coupling scheme, which is similar to other kinetic-MHD codes like M3D-K(Fu *et al.* 2006) and NIMROD(Kim 2008). The particle equation of motion, δf equations, and coupling scheme are described in Liu *et al.* (2022). In the new version of M3D-C1-K, we treat both the thermal ions and fast ions as kinetic particles and calculate their dynamics using the PIC method, and electrons are treated using a fluid model. The MHD equations with kinetic coupling are as follows,

$$\rho \left[\frac{\partial \mathbf{v}_\perp}{\partial t} + (\mathbf{v}_\perp + \mathbf{v}_\parallel \mathbf{b}) \cdot \nabla \mathbf{v}_\perp \right] = \mathbf{J} \times \mathbf{B} - \nabla_\perp p_e - \nabla_\perp \cdot [P_{i\parallel} \mathbf{b}\mathbf{b} + P_{i\perp} (\mathbf{I} - \mathbf{b}\mathbf{b})] \\ - \nabla_\perp \cdot [P_{f\parallel} \mathbf{b}\mathbf{b} + P_{f\perp} (\mathbf{I} - \mathbf{b}\mathbf{b})] + \nu \nabla^2 \mathbf{v}_\perp, \quad (2.1)$$

$$\mathbf{J} = \frac{1}{\mu_0} \nabla \times \mathbf{B}, \quad (2.2)$$

$$\frac{\partial \mathbf{B}}{\partial t} = -\nabla \times \mathbf{E}, \quad (2.3)$$

$$\mathbf{E} = -\mathbf{v}_\perp \times \mathbf{B} + \eta \mathbf{J}. \quad (2.4)$$

Here ρ is the total ion mass density, \mathbf{v}_\parallel and \mathbf{v}_\perp are the MHD velocity parallel and perpendicular to the magnetic field \mathbf{B} , \mathbf{J} is the plasma current density, \mathbf{E} is the electric field, ν and η are viscosity and resistivity coefficients. \mathbf{P}_\parallel and \mathbf{P}_\perp are the parallel and perpendicular components of the ion pressure tensor, and the subscript i and f represents thermal ion and fast ions. The electron pressure p_e can either be calculated with the convection and diffusion terms,

$$\frac{\partial p_e}{\partial t} + (\mathbf{v}_\perp + \mathbf{v}_\parallel \mathbf{b}) \cdot \nabla p_e = -\gamma_e p_e \nabla \cdot [(\mathbf{v}_\perp + \mathbf{v}_\parallel \mathbf{b})] + n_e \nabla \cdot [\kappa_\perp \mathbf{I} + \kappa_\parallel \mathbf{b}\mathbf{b}] \cdot \nabla \left(\frac{p_e}{n_e} \right), \quad (2.5)$$

or as a product of density and electron temperature ($p_e = n_e T_e$). The temperature can be calculated separately

$$\frac{\partial T_e}{\partial t} + (\mathbf{v}_\perp + \mathbf{v}_\parallel \mathbf{b}) \cdot \nabla T_e = -(\gamma_e - 1) T_e \nabla \cdot [(\mathbf{v}_\perp + \mathbf{v}_\parallel \mathbf{b})] + \nabla \cdot [\kappa_\perp \mathbf{I} + \kappa_\parallel \mathbf{b}\mathbf{b}] \cdot \nabla T_e, \quad (2.6)$$

where γ_e is the electron specific heat ratio, κ_\parallel and κ_\perp are the parallel and perpendicular heat transport coefficients.

The kinetic ion orbit follows the guiding-center equation of motion,

$$\frac{d\mathbf{X}}{dt} = \frac{1}{B^\star} \left[V_\parallel \mathbf{B}^\star - \mathbf{b} \times \left(\mathbf{E} - \frac{\mu}{q} \nabla B \right) \right], \quad (2.7)$$

$$m \frac{dV_\parallel}{dt} = \frac{1}{B^\star} \mathbf{B}^\star \cdot (q\mathbf{E} - \mu \nabla B), \quad (2.8)$$

where

$$\mathbf{B}^\star = \mathbf{B} + \frac{mV_\parallel}{q} \nabla \times \mathbf{b}, \quad (2.9)$$

$$\mathbf{B}^\star = \mathbf{B}^\star \cdot \mathbf{b}. \quad (2.10)$$

$$\mathbf{E}^\star = \mathbf{E} - \frac{1}{n_e e} \nabla_{\parallel} p_e. \quad (2.11)$$

Here \mathbf{X} is the particle guiding center location, V_{\parallel} the the particle parallel velocity. m is the ion mass. $\mu = mV_{\perp}^2/2B$ is the magnetic moment. $\mathbf{b} = \mathbf{B}/B$. Note that the electric field \mathbf{E}^\star has an additional term in the parallel direction, $-\nabla_{\parallel} p_e/n_e e$. This term is obtained by ignoring the inertial term in the electron momentum equation in the parallel direction.

Assuming that the ion distribution is given as a function of location \mathbf{X} , energy $\mathcal{E} = (1/2)mV^2$ and pitch angle $\xi = V_{\parallel}/V$, the weight equation for δf calculation is obtained from drift kinetic equations,

$$\frac{dw}{dt} = -\alpha \left[\left(\frac{d\mathbf{X}}{dt} \right)_1 \cdot \nabla + \left(\frac{d\mathcal{E}}{dt} \right)_1 \frac{\partial}{\partial \mathcal{E}} + \left(\frac{d\xi}{dt} \right)_1 \frac{\partial}{\partial \xi} \right] \ln f_0, \quad (2.12)$$

where

$$\left(\frac{d\mathbf{X}}{dt} \right)_1 = \frac{\mathbf{E} \times \mathbf{B}}{B^2} + V_{\parallel} \delta \mathbf{b}, \quad (2.13)$$

$$\left(\frac{d\mathcal{E}}{dt} \right)_1 = \left[V_{\parallel} \mathbf{b} + \frac{mV_{\parallel}^2}{qB} \mathbf{b} \cdot \nabla \times \mathbf{b} + \frac{\mu}{qB} \mathbf{b} \times \nabla B \right] \cdot q\mathbf{E}^\star, \quad (2.14)$$

$$\left(\frac{d\xi}{dt} \right)_1 = \frac{1}{V} \frac{dV_{\parallel}}{dt} - \frac{2V_{\parallel}}{mV^3} \frac{d\mathcal{E}}{dt}, \quad (2.15)$$

$$\left(\frac{dV_{\parallel}}{dt} \right)_1 = \left[\mathbf{b} + \frac{mV_{\parallel}}{qB} \nabla \times \mathbf{b} \right] \cdot \frac{q}{m} \mathbf{E}^\star + \delta \mathbf{b} \cdot \left(-\frac{\mu}{m} \nabla B \right). \quad (2.16)$$

$\alpha = 1$ for linear calculation and $\alpha = 1 - w$ for nonlinear. Alternatively, one can calculate the difference between the results of the equations of motion with equilibrium and perturbed fields to obtain these $(\dots)_1$ terms.

Finally, the density, parallel velocity and pressure for thermal (subscript i) and fast (subscript f) ions used in the MHD equations are calculated from particle deposition on fields,

$$\delta n_{i,f}(\mathbf{x}) = \sum_{k_{i,f}} \left(w_{k_{i,f}} + \frac{\delta B_{\parallel}}{B_0^\star} \right) S(\mathbf{x} - \mathbf{x}_{k_{i,f}}), \quad (2.17)$$

$$\delta \rho = m_i \delta n_i + m_f \delta n_f, \quad (2.18)$$

$$\delta n_e = Z_i \delta n_i + Z_f \delta n_f, \quad (2.19)$$

$$\begin{aligned} \delta v_{\parallel}(\mathbf{x}) = \frac{1}{n_{e0} + \delta n_e} & \left[\sum_{k_i} Z_i V_{\parallel, k_i} \left(w_{k_i} + \frac{\delta B_{\parallel}}{B_0^\star} \right) S(\mathbf{x} - \mathbf{x}_k) - Z_i n_{i0} v_{\parallel, i, 0} \right. \\ & \left. + \sum_{k_f} Z_f V_{\parallel, k_f} \left(w_{k_f} + \frac{\delta B_{\parallel}}{B_0^\star} \right) S(\mathbf{x} - \mathbf{x}_k) - Z_f n_{f0} v_{\parallel, f, 0} \right], \end{aligned} \quad (2.20)$$

$$\delta P_{\parallel i,f}(\mathbf{x}) = \sum_{k_{i,f}} m_{i,f} V_{\parallel,k_{i,f}}^2 \left(w_{k_{i,f}} + \frac{\delta B_{\parallel}}{B_0^*} \right) S(\mathbf{x} - \mathbf{x}_{k_{i,f}}), \quad (2.21)$$

$$\delta P_{\perp i,f}(\mathbf{x}) = \sum_{k_{i,f}} \mu_{k_{i,f}} B_0 \left(w_{k_{i,f}} + \frac{\delta B_{\parallel}}{B_0^*} + \frac{\delta B_{\parallel}}{B_0} \right) S(\mathbf{x} - \mathbf{x}_{k_{i,f}}) \quad (2.22)$$

Here S is the particle shape function, $k_{i,f}$ are index of particles, m_i and m_f are the ion mass, Z_i and Z_f are ion effective charge, $v_{\parallel 0}$ is the parallel velocity of ion equilibrium distribution f_0 . The details of the implementation of the particle deposition calculation can be found in Liu *et al.* (2022). For simulation with finite Larmor radius (FLR) effects, both the field evaluation and the particle deposition need to take into account average along the gyro orbit.

The kinetic-MHD scheme here is similar to that implemented in MEGA(Sato & Todo 2019, 2020), except that we use pressure coupling while MEGA uses current coupling. As pointed out in Liu *et al.* (2022), the two kinds of coupling schemes are equivalent for calculating v_{\perp} . Comparing with the pressure coupling scheme with thermal ions in Park *et al.* (1999), we have additional equations for synchronization of ion density and parallel velocity with MHD fields, whereas in Park *et al.* (1999) these quantities are calculated by the MHD equations. For example, the parallel velocity is solved as

$$\begin{aligned} \rho \left[\frac{\partial v_{\parallel}}{\partial t} + (\mathbf{v}_{\perp} + v_{\parallel} \mathbf{b}) \cdot \nabla v_{\parallel} \right] = & -\nabla_{\parallel} \cdot [P_{i\parallel} \mathbf{b}\mathbf{b} + P_{i\perp} (\mathbf{I} - \mathbf{b}\mathbf{b})] \\ & -\nabla_{\parallel} \cdot [P_{f\parallel} \mathbf{b}\mathbf{b} + P_{f\perp} (\mathbf{I} - \mathbf{b}\mathbf{b})] - \nabla_{\parallel} p_e. \end{aligned} \quad (2.23)$$

If assuming small ion energy and ignoring the gradient and curvature drifts, one can verify that Eq. (2.23) can be obtained by taking the moment of kinetic equations. Here $\nabla_{\parallel} p_e$ is derived from the parallel electric field term in Eq. (2.11) which is used in particle weight equations. In principle, the pressure coupling scheme in Park *et al.* (1999) is equivalent to our coupling scheme and the simulation results should agree with each other, though the calculation of ion density and v_{\parallel} in MHD equations are redundant.

However, we find that in M3D-C1, due to the fact that the fluid equations and kinetic equations are solved subsequently in one timestep, in the simulation using the scheme of Park *et al.* (1999), the difference between δn and δv_{\parallel} from the fluid and kinetic equations can increase with time, which violates the quasi neutrality condition and lead to parasitic modes that overwhelm the numerical result. We thus replace the two MHD equations with the synchronization schemes instead to avoid these issues. The perpendicular momentum equation (Eq. (2.1)) of MHD is kept as it provides additional information for kinetic simulation. In fact, Eq. (2.1) can be regarded as a decomposition of plasma perpendicular current, in which $\rho \partial \mathbf{v}_{\perp} / \partial t$ term represents the polarization current, and the pressure terms represent the drift and magnetization current.

The ion's parallel velocity is used in the electron pressure (Eq. (2.5)) and temperature equation (Eq. (2.6)), assuming that the electrons and ions are moving together. However, when considering two-fluid effects, there is a difference between the electron and ion velocities due to the parallel current. This difference can leads to correction terms in Eq. (2.5) and Eq. (2.6) that are proportional to d_i/L (d_i is the ion skin depth), and thus can be considered as a two-fluid term. These two-fluid terms are ignored in the current simulation model as we are dealing with long-wavelength modes. The additional parallel electric field used in Eq. (2.11) is not included in the Ohm's law (Eq. (2.4)) for the same

reason. These two-fluid effects can be important for high- k mode simulations like kinetic Alfvén wave (KAW), and will be studied in future.

3. Numerical simulation of ion acoustic wave

In this section we test the new version of M3D-C1-K in an IAW simulation. The oscillation of IAWs can be easily simulated using a MHD code. However, for $T_i \sim T_e$, IAW will be strongly damped due to parallel Landau damping, which can only be simulated by including the kinetic effects of thermal ions.

In the simulation we treat thermal ions as kinetic particles and electrons as a fluid component. Since IAW is an electrostatic mode, we only keep the MHD equation Eq. (2.5) and ignore the v_\perp terms. The MHD equation and the particle equation of motion are limited to one-dimensional along the wave vector. For electron pressure we choose the electron heat capacity ratio $\gamma_e = 1$ assuming they are isothermal. The parallel velocity is initialized like a sinusoidal function with a fixed wave number k , which can drive perturbations on p_e and p_i and lead to a standing wave. The electron and ion density are the same assuming $Z_{\text{eff}} = 1$, and the ion temperature is set to be a fraction of electron temperature.

For MHD-only simulation, we find that IAW gives oscillations of δp and δv_\parallel with little damping. With ion kinetic effects, the oscillation experiences damping as shown in Fig. 1. We find that the mode damping rate is consistent with the theoretical Landau damping rate of IAW which is shown as the red line. Note that for $T_i/T_e > 0.1$, the Landau damping rates γ_{LD} of IAWs become comparable to ω and the perturbative calculation is not accurate. In these cases γ_{LD} should be solved numerically from the plasma dispersion function $Z(\zeta)$. Here we use empirical functions to calculate the frequencies and the Landau damping rates of IAWs for $0.1 < T_i/T_e < 1$ from Chen (2013),

$$\omega = \omega_0 \sqrt{1 + \frac{3T_i}{T_e}} \quad (3.1)$$

$$\frac{\gamma_{LD}}{\omega} = 1.1 * \left(\frac{T_i}{T_e}\right)^{7/4} \exp \left[- \left(\frac{T_i}{T_e}\right)^2 \right] \quad (3.2)$$

where $\omega_0 = k\sqrt{k_B T_e/m_i}$ and k_B is the Boltzmann constant. Eq. (3.1) is calculated by assuming the ion heat capacity ratio $\gamma_i = 3$ since they only suffer one-dimension compression (McKinstrie *et al.* 1999; Chen 2013).

Fig. 2 shows the results of IAW frequencies and damping rates from the M3D-C1-K simulation for different values of T_i/T_e . For small T_i/T_e , the damping rate is zero and the frequency is close to the MHD-only result ω_0 . For $T_i/T_e > 0.3$, the damping rate becomes comparable to the frequency indicating IAWs are strongly damped. Both ω and γ_{LD} are close to the theoretical results, indicating that the new kinetic-MHD model successfully captures the Landau damping physics.

We find that for large T_i/T_e , the mode can have echos after being significantly damped, as shown in Fig. 3. This phenomenon is a typical nonlinear behavior for the Landau damped mode, which is different from dissipative damping (Kadomtsev 1968). This effect indicates that although the mode is damped due to phase mixing, the particles still retain some “memory” of the preceding oscillation which can be reflected as echos at later times.

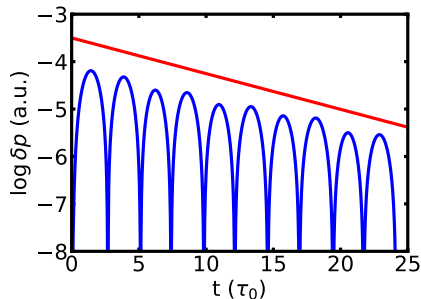


FIGURE 1. Blue line is the time signal of δp_e from IAW simulation with $T_i = 0.2T_e$. Red line shows a mode damping trend with a rate calculated from Eq. (3.2). The time unit $\tau_0 = 1/\omega_0$.

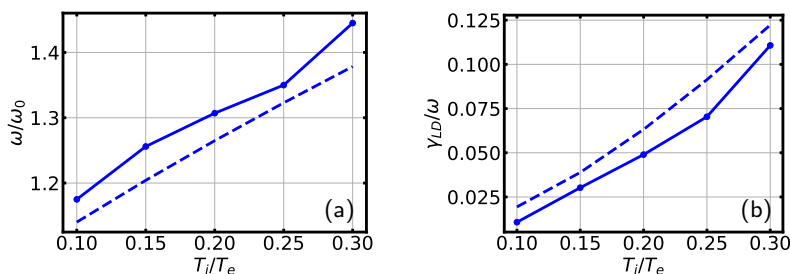


FIGURE 2. Frequencies (a) and damping rates (b) from IAW simulation for different values of T_i/T_e . The dashed lines are the theoretical results calculated from Eq. (3.1) and Eq. (3.2).

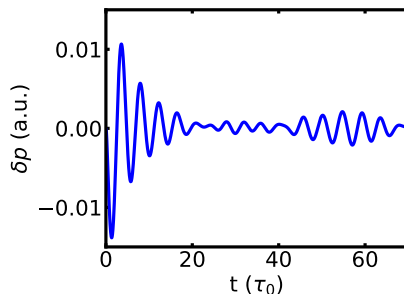


FIGURE 3. Time evolution of δp_e from IAW simulation with $T_i = 0.3T_e$, showing echos of oscillation after the mode damped.

4. Linear simulation of fishbone modes in DIII-D

In this section we discuss the linear $n = 1$ fishbone mode simulation using M3D-C1-K without and with thermal ion kinetic effects. We use an equilibrium from the DIII-D tokamak experiment, obtained from hybrid discharge #125476, which has been studied before for $n = 1$ MHD instabilities using NIMROD (Brennan *et al.* 2012). In the experiment, both a (1,1) kink mode and (2,1) and (3,2) tearing modes are present (La Haye *et al.* 2010). We use a single equilibrium reconstruction from the EFIT code (Lao *et al.* 1990) including motional Stark effect (MSE) profile data, by choosing a time (3425ms) during the stationary phase of the discharge with benign tearing mode excitation. The

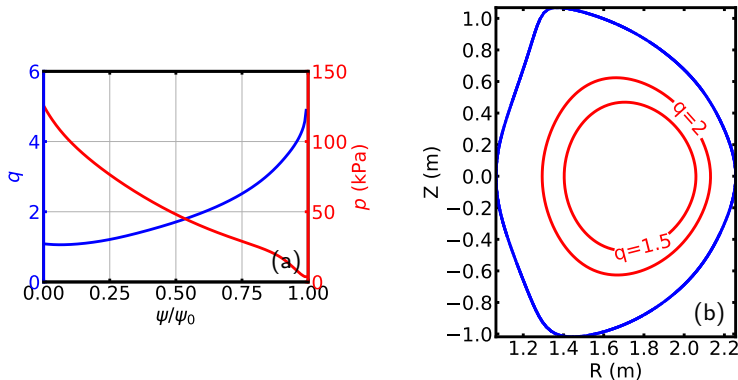


FIGURE 4. (a) Profiles of q and total pressure of the equilibrium used in the DIII-D simulation. (b) Flux contours and mesh boundary used in the simulation.

toroidal flow is not included in the simulation. The equilibrium profiles of q and total pressure, and the shape of flux contours, are shown in Fig. 4. For this equilibrium the safety factor has a minimum $q_{\min} = 1.06$ located at $\psi/\psi_0 = 0.0625$, inside which there is a slightly reverse shear near the core. To study the effect of the q profile on the stability of fishbone modes, we apply the Bateman scaling method (Bateman 1978) to the equilibrium, which means that we add a constant value to F^2 ($F = RB_\phi$) to change the toroidal field while keeping the pressure and the toroidal current fixed and the Grad-Shafranov equation satisfied.

Both thermal ions and fast ions from neutral beam injection are included in the kinetic-MHD simulation. Both of the populations are deuterium. The thermal ions are initialized with Maxwellian distribution, with density $n_i = n_e - n_f$ (n_f is the fast ion density) and temperature $T_i = T_e$. The fast ions have a slowing-down distribution in energy with isotropic distribution in pitch angle,

$$f_0 = \frac{n_f(\psi)}{\mathcal{E}^{3/2} + \mathcal{E}_c^{3/2}}, \quad (4.1)$$

where $\mathcal{E}_c = 10\text{keV}$ is the critical energy. f_0 has a cutoff energy $\mathcal{E}_{\max} = 50\text{keV}$. Both \mathcal{E}_c and \mathcal{E}_{\max} are constants in the simulation domain. The density of the fast ions n_f has the same profile as the total pressure, so that the fraction of fast ion pressure to the total pressure is fixed (16%) at different flux surfaces.

For linear simulations, we use a two-dimensional finite element mesh and a spectral representation of the MHD fields in the toroidal direction. The 2D unstructured mesh has 5495 triangular elements which are uniformly distributed. For the kinetic-MHD simulation we use 8×10^6 particle markers, half of which are for the simulation of fast ions and the other half for the thermal ions.

The simulation results of mode growth rates and frequencies are summarized in Fig. 5, with q_{\min} varying from 1.0 to 1.2. The MHD-only result (blue line) shows that the $n = 1$ kink mode is unstable for $q_{\min} < 1.06$. After including the fast ion kinetic effects (red lines), the mode growth rates decrease for the $q_{\min} < 1.04$, and the modes have finite frequencies due to the wave-particle resonances, which increase with q_{\min} . For $q_{\min} > 1.1$, there is still a weakly unstable $n = 1$ mode which is driven by fast ions, with frequencies significantly larger than those of $q_{\min} < 1.06$ cases. The manifest change of frequencies indicates that the dominant $n = 1$ mode changes from a fishbone-like branch to a BAE-

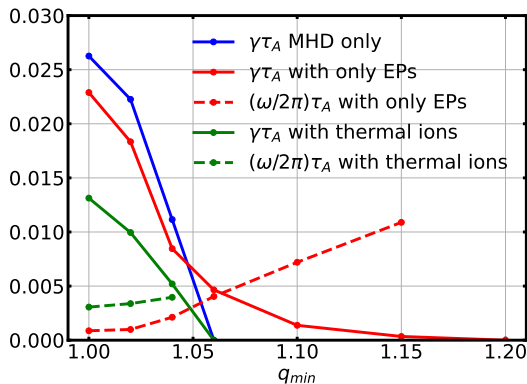


FIGURE 5. Growth rates (solid lines) and frequencies (dashed lines) as functions of q_{\min} of the $n = 1$ mode from M3D-C1 linear simulations with DIII-D equilibrium. The blue lines shows the MHD-only result. The red lines show the kinetic-MHD results with only fast ions. The green lines show the results with both thermal and energetic ions.

like branch with distinct frequencies. The results of the mode frequencies and growth rates are close to the NIMROD results in Brennan *et al.* (2012), except that the growth rate for $q_{\min} > 1.1$ keeps dropping to zero as q_{\min} increases, whereas in Brennan *et al.* (2012) the growth rate is almost a constant for large q_{\min} .

The 2D structure of the fishbone mode for $q_{\min} = 1.04$ including thermal ions is summarized in Fig. 6-9. Fig. 6 shows the mode structure of perturbed velocity stream function ($\delta\phi$) and magnetic flux ($\delta\psi$). $\delta\phi$ is dominated by $m = 1$ near the core and $m = 2$ at the outer region, and $\delta\psi$ is dominated by $m = 2$. Fig. 7 shows the structure of electron and ion pressure, which is similar to the $\delta\phi$ structure. The similarity between δp_e and δp_i indicates that the quasi-neutrality condition is satisfied. Fig. 8 shows the structure of fast ion pressure, including parallel and perpendicular components in Eqs. (2.21) and (2.22). The non adiabatic response ($\delta p_{\perp} - \delta p_{\parallel}$) is mostly located in the low-field side, as it comes from the resonant trapped particles (Fu *et al.* 2006; Kim 2008; Liu *et al.* 2022). Fig. 9 shows the comparison of δv_{\parallel} from the kinetic-MHD simulation using parallel velocity synchronization (Eq. (2.20)), with the result of the simulation with only fast ions and no synchronization. The two results are close and both are dominated by $m = 2$, showing that the kinetic equations successfully captures the parallel dynamics of the MHD system.

According to the simulation results, we find that both the fishbone branch and the BAE-like branch of the $n = 1$ mode are susceptible to Landau damping of thermal ions. The parallel wave number can be estimated as follows,

$$k_{\parallel} \approx \frac{1}{R} \left(n - \frac{m}{q_{\min}} \right). \quad (4.2)$$

Here we choose $m = 1.5$ as the mode has both $m = 1$ and $m = 2$ components. Using the mode frequency obtained from simulation with fast ions, for $q_{\min} = 1.04$ there is $\omega/k_{\parallel} = 0.20v_{\text{th}}$, and for $q_{\min} = 1.15$, there is $\omega/k_{\parallel} = 1.15v_{\text{th}}$, where $v_{\text{th}} = \sqrt{T_i/m_i}$. Therefore the Landau damping effects are important for both branches, which explains the stabilization of the mode by thermal ions for $q_{\min} > 1.06$ cases providing their small growth rates without thermal ions. It is necessary to include the thermal ion kinetic effects and Landau damping in those case to avoid false positive results.

In the above study we scan the value of q_{\min} by varying the toroidal field and keep the plasma pressure fixed. This can leads to change to both q_{\min} and plasma β at the

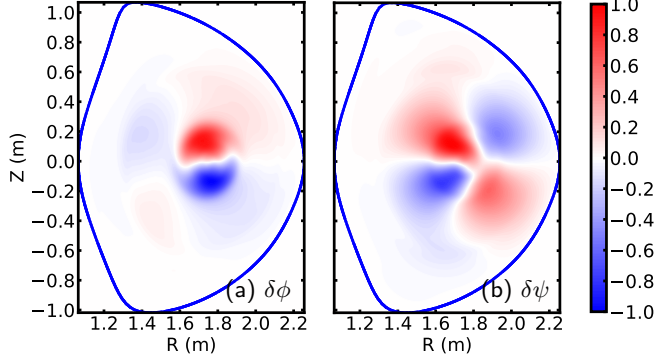


FIGURE 6. 2D structure of $\delta\phi$ (a) and $\delta\psi$ (b) from DIII-D $n = 1$ linear simulation of the $q_{\min} = 1.04$ case with thermal ions.

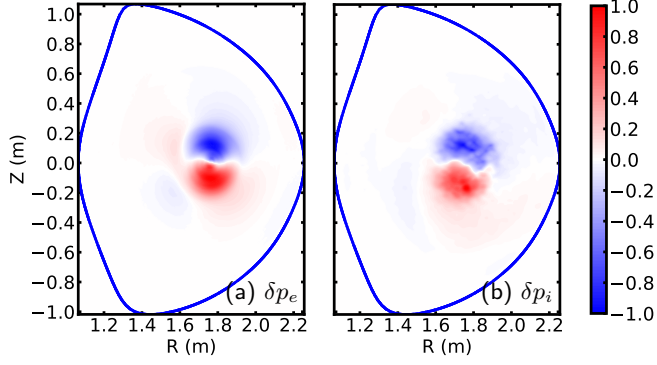


FIGURE 7. 2D structure of perturbed electron pressure δp_e (a) and thermal ion pressure δp_i (b) from the linear simulation of the $q_{\min} = 1.04$ case with thermal ions.

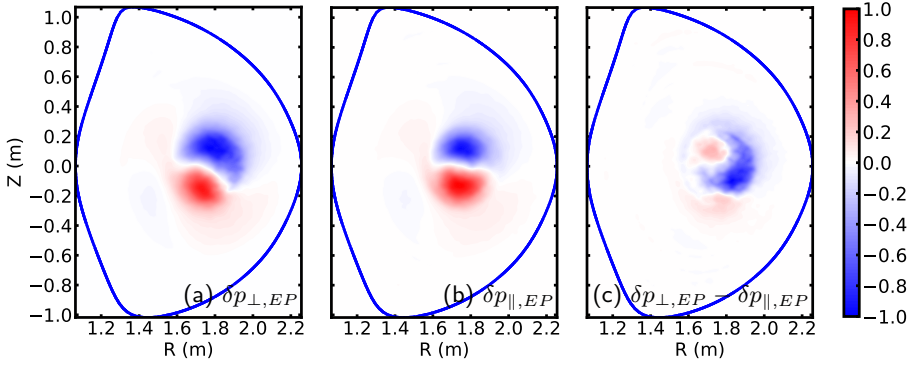


FIGURE 8. 2D structure of perpendicular (a) and parallel (b) fast ion pressure from the linear simulation of the $q_{\min} = 1.04$ case with thermal ions, and the difference between the two (c).

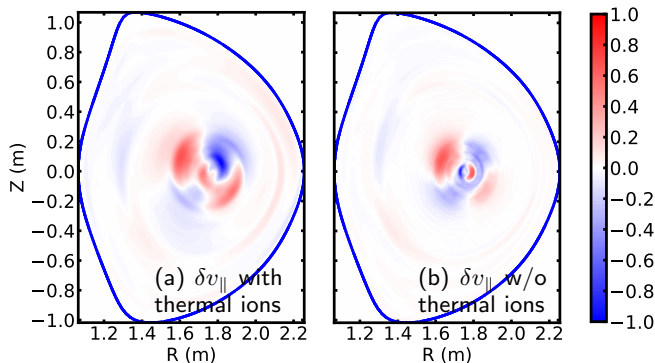


FIGURE 9. (a) Structure of v_{\parallel} from the linear simulation of the $q_{\min} = 1.04$ case with thermal ions and synchronization of v_{\parallel} (Eq. (2.20)). (b) Structure of v_{\parallel} from the linear simulation with only fast ions using MHD equation Eq. (2.23).

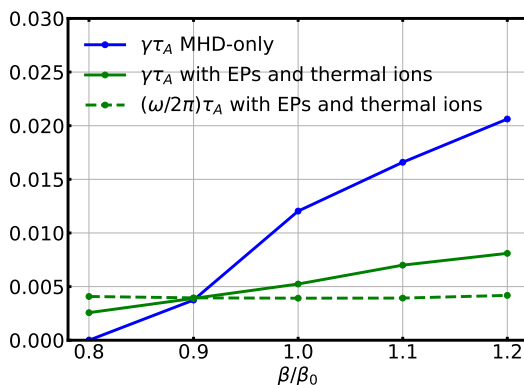


FIGURE 10. Growth rates (solid lines) and frequencies (dashed lines) of the $n = 1$ mode with different plasma β (β_0 is the experimental value) and a fixed q profile. The blue lines shows the MHD-only result. The green lines show the kinetic-MHD results with fast and thermal ions.

same time, as discussed in Brennan *et al.* (2012). To separate the two effects, we rerun the reconstruction of the equilibrium by fixing the toroidal field and q profile while scaling the total pressure, by varying T_e , T_i and fast ion energy. The results of MHD-only simulations and simulations with fast ion and thermal ion kinetic effects are summarized in Fig. 10, with $q_{\min} = 1.04$. The results indicate that, although the (1,1) mode bears the name “non-resonant kink (NRK) mode” in some literature (Wang *et al.* 2013), its growth rate has a strong dependence on the plasma beta value, especially for the MHD-only simulations, which is similar to pressure-driven modes. After including ion kinetic effects, the dependence of growth rate on β weakens, and the mode frequency is almost independent of β .

With the Landau damping effect included, the $n = 1$ mode is stable for $q_{\min} > 1.06$. For the original equilibrium from EFIT, $q_{\min} = 1.06$, the mode is at the stability boundary, which may be the result of nonlinear evolution of fishbone mode and the flattening of the current profile near the core. The fishbone-like mode in the simulation with $q_{\min} = 1.04$ has a frequency about $f = 6.13$ kHz. In the DIII-D experiment, the dominant $n = 1$ mode is identified to have a frequency of 18 kHz in the lab frame, and the toroidal rotate

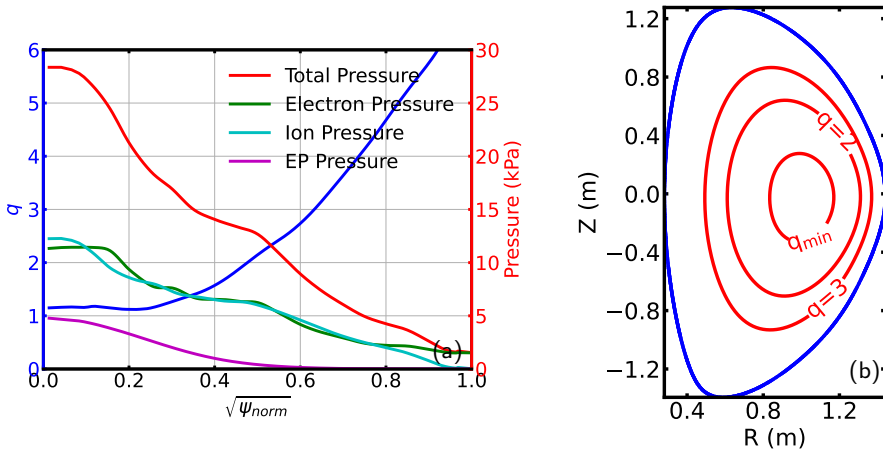


FIGURE 11. (a) Profiles of q and pressure of different particle species of the equilibrium used in the NSTX simulation. (b) Flux contours and mesh boundary used in the simulation.

frequency is about 21 kHz. Therefore the simulation of fishbone-like mode is consistent with the measured frequency in the plasma frame.

5. Linear simulation of fishbone modes in NSTX

We did a similar study for the $n = 1$ mode under a NSTX experimental condition. The equilibrium q profile is obtained from NSTX shot #134020 at 700ms. The density and temperature profiles are from the TRANSP(Ongena *et al.* 2012) calculation result. The Grad-Shafranov (G-S) equation was solved using these profiles in a M3D-C1 2D mesh with 7199 elements. We ignored the contribution of high- Z impurities and assume all the ions are deuterium. The profiles used in the simulation and the shape of flux contours are shown in Fig. 11. The core electron density is $1.04 \times 10^{20} \text{m}^{-3}$, and the core electron and ion temperature is about 0.74 keV. The ratio of EP beta to the total beta at core is $\beta_{EP}/\beta = 17.3\%$. Note that a key difference from the DIII-D equilibrium is that NSTX has much large plasma β ($\beta_{on-axis} = 50.8\%$ vs. DIII-D $\beta_{on-axis} = 12.4\%$). In the NSTX simulation we use Spitzer resistivity calculated from local electron temperature, and apply a large value of parallel heat conduction coefficient $\kappa_{||}$.

For EP we use an anisotropic distribution from the NUBEAM calculation. The NUBEAM code provides 3D (r , $\lambda = V_{||}/V$, energy) information of injected beam ions from Monte Carlo calculation(Pankin *et al.* 2004), which is called the classical fast ion distribution. The NUBEAM distribution near the magnetic axis (Fig. 12 (a)) shows that the lower energy EPs ($\mathcal{E} < 40 \text{keV}$) are mostly co-passing with $V_{||}/V \approx 1$, and the higher energy EPs have a peak distribution at $V_{||}/V \approx 0.4$. This initial distribution is quite noisy, making it difficult to calculate the gradients of f_0 in the phase space. In order to use it for δf calculation, we apply a Gaussian smoothing operator to obtain a smoothed distribution as shown in Fig. 12 (b). This new distribution is then read into M3D-C1-K as f_0 and used for both particle initialization and δf calculation. The radial profile of EP pressure is shown in Fig. 11, which is consistent with the TRANSP output.

In terms of the shortcomings of Bateman scaling method, and the sensitive dependence of $n = 1$ mode growth rate on β as discussed in Sec. 4, for NSTX we apply a new method to scan the value of q_{min} , by fixing the toroidal field and changing the plasma current

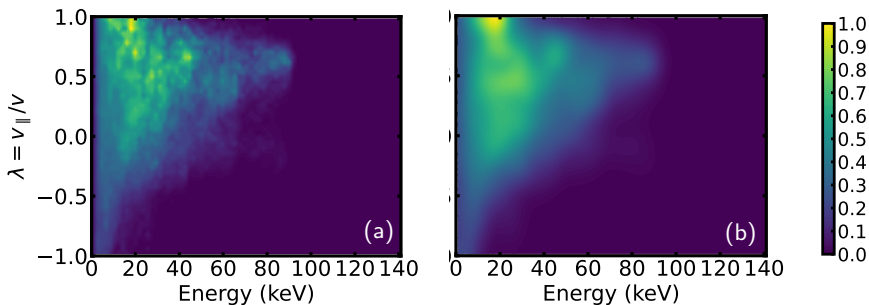


FIGURE 12. (a) The original EP distribution of energy and pitch angle near the magnetic axis from NUBEAM. (b) The smoothed EP distribution that was used in M3D-C1-K simulations.

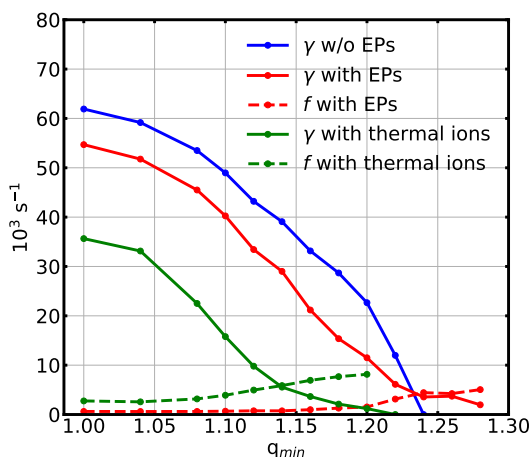


FIGURE 13. Growth rates γ (solid lines) and frequencies f (dashed lines, in kHz) as functions of q_{\min} of the $n = 1$ modes from M3D-C1 linear simulation with NSTX equilibrium with fixed β . The blue line shows the MHD-only result. The red lines show the kinetic-MHD results with only fast ions. The green lines show the results with both thermal and energetic ions.

to fit the new q profile. This method ensures that β is almost fixed when scanning q_{\min} . The results of kinetic-MHD and MHD-only $n = 1$ linear simulations are summarized in Fig. 13. The threshold value of q_{\min} for $n = 1$ mode excitation is higher than the DIII-D results, thanks to the larger β . For kinetic-MHD simulations with only fast ions (red lines), the dominant mode changes from fishbone-like to BAE-like as q_{\min} increases above 1.2, with an increase of mode frequencies.

After including the thermal ion kinetic effects, the frequencies of fishbone-like modes increase significantly, while the growth rates decrease because of Landau damping. It is known that the fishbone mode is driven by the trapped ions which can have resonances with the mode through precession motion. However, as shown in Fig. 12, the population of trapped particles ($\lambda \approx 0$) in fast ions is relatively small compared to the co-passing ions, which leads to the low frequency of the fishbone-like modes. The thermal ions, on the other hand, have an isotropic distribution and can provide a large population of trapped ions to drive the fishbone-like mode. The mode structure of the fishbone-like

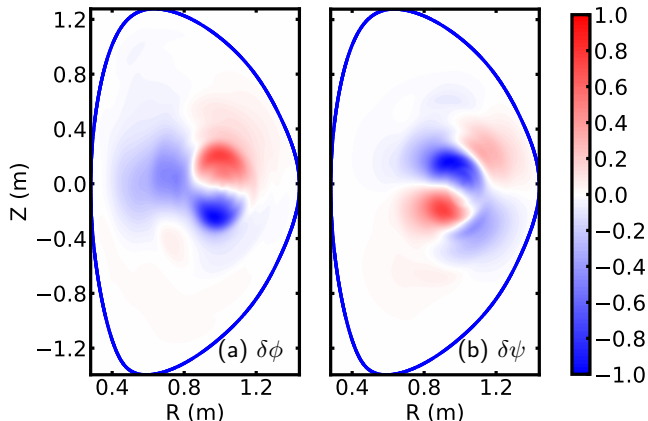


FIGURE 14. 2D structure of $\delta\phi$ (a) and $\delta\psi$ (b) from NSTX $n = 1$ linear simulation of the $q_{\min} = 1.12$ case with thermal ions.

mode for $q_{\min} = 1.12$ is shown in Fig. 14. For $q_{\min} > 1.22$, the Landau damping effect stabilizes the BAE-like mode, which is similar to the DIII-D results.

In the NSTX experiment, both the kink ($m = 1$) and tearing ($m = 2$) modes have been identified using soft x-ray diagnostics, and the synergy effect of the two modes can lead to fast ion transport (Yang *et al.* 2021). It is believed that the $m = 2$ mode is mainly neoclassical tearing mode (NTM) which is affected by the current associated with EPs. The $m = 1$ mode is marginally unstable in M3D-C1-K simulation with thermal ions under the experimental condition ($1.1 < q_{\min} < 1.2$), similar to the DIII-D case, which may be a result of pressure and current relaxation due to the nonlinear saturation of fishbone mode. The frequency observed in experiment is less than 5kHz after subtracting the Doppler frequency of toroidal rotation, which is close to the simulation frequency with $q_{\min} = 1.12$. Note that the oscillation frequency after nonlinear saturation can be lower than the linear result due to the down-chirping of fishbone mode.

6. Nonlinear simulation of fishbone-like mode in NSTX

Based on the linear simulation, we conduct the nonlinear simulation of the $n = 1$ fishbone-like mode including the thermal ion kinetic effects in NSTX. We use the same MHD equilibrium and EP distribution as in Sec. 5, with $q_{\min} = 1.12$. The simulation utilized a 3D finite element mesh, and nonlinear terms are included in the MHD and δf equations. The mesh has 8 toroidal planes connected by Hermite finite elements in the toroidal direction, which is good enough to resolve the $n = 1$ perturbation, as we focus on the growth and saturation of the $n = 1$ mode and its nonlinear coupling with the $n = 0$ mode in this simulation. The mesh structure of each plane is the same as in the linear simulation. We use 16×10^6 particle markers for the PIC simulation.

The nonlinear simulation was conducted at Perlmutter cluster at NERSC. For each nonlinear simulation we use 8 nodes with 64 AMD cores and 4 NVIDIA Tesla A100 GPUs on each node. The GPUs are used to do the MHD equation matrix element calculation and particle pushing. The CPU was used to solve the matrix by calling PETSC library, and calculate the particle moments.

The time evolution of the kinetic and magnetic parts of the MHD energy in the nonlinear NSTX fishbone simulation is shown in Fig. 15. We find that the $n = 1$ mode

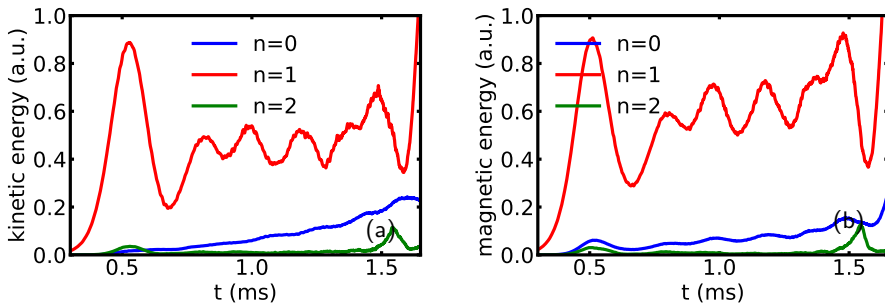


FIGURE 15. Time evolution of kinetic energy (a) and magnetic energy (b) of different toroidal harmonics from NSTX nonlinear simulation of the $q_{\min} = 1.12$ case with thermal ions.

reaches a saturation point at about $t = 0.5$ ms. The peak $\delta B/B_0$ at this point is about 1.5×10^{-2} . There is also a $n = 0$ mode excited due to the nonlinear mode-mode coupling. After the saturation, the magnetic energy of the $n = 1$ mode stays at a high level, and the energy of $n = 0$ mode keeps growing, meaning that the change to the magnetic field topology does not decay. The Poincaré plot of magnetic flux after mode saturation ($t = 1.2$ ms) is shown in Fig. 16 (a). There is a clear shift of the magnetic axis due to the excitation of (1,1) mode. The kink boundary overlaps with the flux contour of $q = q_{\min}$, meaning that most of the magnetic perturbation happens in the reversed-shear region. Although the equilibrium has $q > 1.12$, the excitation of the mode creates a (1,1) island near the magnetic axis, and (2,1) islands near the $q = 2$ surface, which is consistent with the experimental observation.

The growth of the $n = 1$ mode can lead to transport of EPs. Fig. 16 (b) shows the flux-averaged profiles of EP density before and after mode saturation. This result shows that although the $n = 1$ mode can provide a large δB field, it only leads to a slight drop of EP density (about 5%) near the axis. The profile gradient does not drop to zero after saturation because the mode is susceptible to Landau damping, which means that it requires a finite radial gradient to excite. However, Fig. 16 (b) is a flux-averaged result and does not show the change of gradient along the mode's resonance line in phase space, which may be more significant.

7. Summary

The new kinetic-MHD simulation approach in this paper includes all the ions as kinetic particles, which is different from the classical approach that only deals with kinetic effects of fast ions. To implement that, part of the MHD equations, the density equation and the parallel velocity equation, are replaced by synchronization from kinetic particle simulation, to avoid redundant calculation and parasitic modes caused by numerical errors. The rest of the MHD equations can still be solved using a semi-implicit method with large timestep, which is different from the fully-kinetic or gyrokinetic simulation approach. The inclusion of thermal ion kinetic effects is important for macroscopic instability simulations targeting ITER and fusion reactors with large ion temperature.

The new simulation method has been used to study the thermal ion Landau damping of IAWs and fishbone modes. It is found that the $n = 1$ fishbone modes driven in an equilibrium with $q_{\min} > 1$, or non-resonant fishbone modes, can be strongly affected by the Landau damping effects, since the mode phase velocity in the parallel direction is of the same order as the ion thermal velocity. In the linear simulation using a DIII-D and

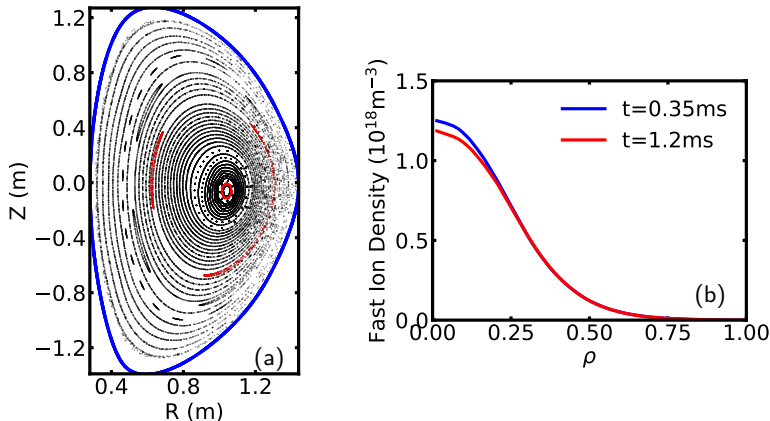


FIGURE 16. (a) Poincaré plot of magnetic flux surfaces at $t = 1.2\text{ms}$. (1,1) and (2,1) islands are marked as red. (b) Change of fast ion density profile in the nonlinear simulation of $q_{\min} = 1.12$ due to mode excitation.

NSTX equilibrium, it is found that the $n = 1$ BAE-like modes driven by fast ions can be stabilized by the thermal ions. Therefore it is necessary to revisit those non-resonant fishbone simulations done by kinetic-MHD codes, and add the thermal ion kinetic effects.

In developing the kinetic-MHD method, we include the parallel electric field calculated from electron pressure in the kinetic equations, which is essential for the IAW simulation. This term however is not included in the MHD equations. The two-fluid terms, including the parallel and perpendicular electric fields driven by Hall terms and electron pressure, can be important for the calculation of plasma waves with wavelength comparable to ion skin depth, such as KAWs and whistler waves. The two-fluid terms have been developed in M3D-C1 and used to calculate their effects on magnetic reconnection (Beidler *et al.* 2016), but the simulation with them requires further testing and improvement of the matrix solver. We plan to do simulations with electric fields in both fluid and kinetic equations, to study the two fluid effects self-consistently in future work.

Acknowledgments

We would like to thank Yasushi Todo, Masahiko Sato, Ruirui Ma, Feng Wang, Xiaolong Zhu, Zhihong Lin, Guillaume Brochard, Ge Dong and Chalson Kim for fruitful discussion. This work was supported by US Department of Energy grants DE-AC02-09CH11466. This research used the Traverse cluster at Princeton University. This research also used the Perlmutter cluster of the National Energy Research Scientific Computing Center (NERSC), using a NERSC NESAP Tier 2 award.

REFERENCES

- BATEMAN, G. 1978 *MHD instabilities*.
 BEIDLER, M. T., CASSAK, P. A., JARDIN, S. C. & FERRARO, N. M. 2016 Local properties of magnetic reconnection in nonlinear resistive- and extended-magnetohydrodynamic toroidal simulations of the sawtooth crash. *Plasma Phys. Control. Fusion* **59** (2), 025007.
 BRENNAN, D. P., KIM, C. C. & HAYE, R. J. L. 2012 Energetic particle effects on $n = 1$ resistive MHD instabilities in a DIII-D hybrid discharge. *Nucl. Fusion* **52** (3), 033004.

- CHEN, F. F. 2013 *Introduction to Plasma Physics and Controlled Fusion: Volume 1: Plasma Physics*. Google-Books-ID: WGbaBwAAQBAJ.
- CHOI, G. J., LIU, P., WEI, X. S., NICOLAU, J. H., DONG, G., ZHANG, W. L., LIN, Z., HEIDBRINK, W. W. & HAHM, T. S. 2021 Gyrokinetic simulation of low-frequency Alfvénic modes in DIII-D tokamak. *Nucl. Fusion* **61** (6), 066007.
- DU, X. D., HONG, R. J., HEIDBRINK, W. W., JIAN, X., WANG, H., EIDIETIS, N. W., VAN ZEELAND, M. A., AUSTIN, M. E., LIU, Y., CROCKER, N. A., RHODES, T. L., SÄRKIMÄKI, K., SNICKER, A., WU, W. & KNOLKER, M. 2021 Multiscale Chirping Modes Driven by Thermal Ions in a Plasma with Reactor-Relevant Ion Temperature. *Phys. Rev. Lett.* **127** (2), 025001.
- FERRARO, N. M. & JARDIN, S. C. 2009 Calculations of two-fluid magnetohydrodynamic axisymmetric steady-states. *J. Comput. Phys.* **228** (20), 7742–7770.
- FU, G. Y., PARK, W., STRAUSS, H. R., BRESLAU, J., CHEN, J., JARDIN, S. & SUGIYAMA, L. E. 2006 Global hybrid simulations of energetic particle effects on the $n=1$ mode in tokamaks: Internal kink and fishbone instability. *Phys. Plasmas* **13** (5), 052517.
- GORELENKOV, N. N., VAN ZEELAND, M. A., BERK, H. L., CROCKER, N. A., DARROW, D., FREDRICKSON, E., FU, G.-Y., HEIDBRINK, W. W., MENARD, J. & NAZIKIAN, R. 2009 Beta-induced Alfvén-acoustic eigenmodes in National Spherical Torus Experiment and DIII-D driven by beam ions. *Physics of Plasmas* **16** (5), 056107.
- JARDIN, S. C., FERRARO, N., BRESLAU, J. & CHEN, J. 2012 Multiple timescale calculations of sawteeth and other global macroscopic dynamics of tokamak plasmas. *Comput. Sci. Discov.* **5** (1), 014002.
- KADOMTSEV, B. B. 1968 LANDAU DAMPING AND ECHO IN A PLASMA. *Sov. Phys. Usp.* **11** (3), 328.
- KIM, C. C. 2008 Impact of velocity space distribution on hybrid kinetic-magnetohydrodynamic simulation of the (1,1) mode. *Physics of Plasmas (1994-present)* **15** (7), 072507.
- LA HAYE, R. J., BRENNAN, D. P., BUTTERY, R. J. & GERHARDT, S. P. 2010 Islands in the stream: The effect of plasma flow on tearing stability. *Physics of Plasmas* **17** (5), 056110.
- LAO, L. L., FERRON, J. R., GROEBNER, R. J., HOWL, W., JOHN, H. S., STRAIT, E. J. & TAYLOR, T. S. 1990 Equilibrium analysis of current profiles in tokamaks. *Nucl. Fusion* **30** (6), 1035–1049.
- LIU, C., JARDIN, S. C., QIN, H., XIAO, J., FERRARO, N. M. & BRESLAU, J. 2022 Hybrid simulation of energetic particles interacting with magnetohydrodynamics using a slow manifold algorithm and GPU acceleration. *Comput. Phys. Commun.* **275**, 108313.
- MA, R. R., CHEN, L., ZONCA, F., LI, Y. & QIU, Z. 2021 Theoretical studies of low-frequency Alfvén modes in tokamak plasmas. *Plasma Phys. Control. Fusion*.
- MCKINSTRIE, C. J., GIACONE, R. E. & STARTSEV, E. A. 1999 Accurate formulas for the Landau damping rates of electrostatic waves. *Physics of Plasmas* **6** (2), 463–466.
- ONGENA, J. P. H. E., VOITSEKHOVITCH, I., EVRARD, M. & MCCUNE, D. 2012 Numerical Transport Codes. *Fusion Science and Technology* **61** (2T).
- PANKIN, A., MCCUNE, D., ANDRE, R., BATEMAN, G. & KRITZ, A. 2004 The tokamak Monte Carlo fast ion module NUBEAM in the National Transport Code Collaboration library. *Computer Physics Communications* **159** (3), 157–184.
- PARK, W., BELOVA, E. V., FU, G. Y., TANG, X. Z., STRAUSS, H. R. & SUGIYAMA, L. E. 1999 Plasma simulation studies using multilevel physics models. *Physics of Plasmas* **6** (5), 1796–1803.
- SATO, M. & TODO, Y. 2019 Effect of precession drift motion of trapped thermal ions on ballooning modes in helical plasmas. *Nucl. Fusion* **59** (9), 094003.
- SATO, M. & TODO, Y. 2020 Ion kinetic effects on linear pressure driven magnetohydrodynamic instabilities in helical plasmas. *Journal of Plasma Physics* **86** (3).
- SHEN, W., WANG, F., FU, G. Y., XU, L., LI, G. & LIU, C. 2017 Hybrid simulation of fishbone instabilities in the EAST tokamak. *Nucl. Fusion* **57** (11), 116035.
- SHEN, W., WANG, F., FU, G. Y., XU, L. & REN, Z. 2020 Hybrid simulation of fishbone instabilities with reversed safety factor profile. *Nucl. Fusion* **60** (10), 106016.
- TODO, Y. & SATO, T. 1998 Linear and nonlinear particle-magnetohydrodynamic simulations of the toroidal Alfvén eigenmode. *Phys. Plasmas* **5** (5), 1321–1327.

- WANG, F., FU, G. Y., BRESLAU, J. A. & LIU, J. Y. 2013 Linear stability and nonlinear dynamics of the fishbone mode in spherical tokamaks. *Physics of Plasmas* **20** (10), 102506.
- YANG, J., PODESTÀ, M. & FREDRICKSON, E. D. 2021 Synergy of coupled kink and tearing modes in fast ion transport. *Plasma Phys. Control. Fusion* **63** (4), 045003.